LAWRENCE
LIVERMORE
NATIONAL
LABORATORY

First-principles calculation of mechanical properties of Si <001> nanowires and comparison to nanomechanical theory

B. Lee, R. E. Rudd

October 23, 2006

Disclaimer

First-principles calculation of mechanical properties of Si ⟨001⟩ nanowires and comparison to nanomechanical theory

Byeongchan Lee and Robert E. Rudd[*]

Lawrence Livermore National Laboratory, University of California, L-415, Livermore, California 94551 USA

(Dated: January 26, 2007)

We report the results of first-principles density functional theory calculations of the Young's modulus and other mechanical properties of hydrogen-passivated Si ⟨001⟩ nanowires. The nanowires are taken to have predominantly {100} surfaces, with small {110} facets according to the Wulff shape. The Young's modulus, the equilibrium length and the constrained residual stress of a series of prismatic beams of differing sizes are found to have size dependences that scale like the surface area to volume ratio for all but the smallest beam. The results are compared with a continuum model and the results of classical atomistic calculations based on an empirical potential. We attribute the size dependence to specific physical structures and interactions. In particular, the hydrogen interactions on the surface and the charge density variations within the beam are quantified and used both to parameterize the continuum model and to account for the discrepancies between the two models and the first-principles results.

I. INTRODUCTION

The mechanical response of structures at the nanoscale is known to be different than that of their macroscopic analogs, and surface effects in these high surface-to-volume devices are important.[1] Significant strides forward have been made in the understanding of these effects, but a predictive theory of nanomechanics remains an open problem both at the academic level and in terms of implementation in nanodevice design codes. Nanoscale mechanical devices have been proposed for applications for a range of nanoelectromechanical systems (NEMS). These devices include high-frequency oscillators and filters,[2] nanoscale surface probes,[3] probes of single molecules[4] and spins,[5] nanofluidic valves,[6] and q-bits for quantum computation.[7,8] The process of design and fabrication of these devices is extremely challenging, requiring new techniques for synthesis, characterization, integration and modeling of the device performance that are currently the subject of active research. The process is complicated in part by uncertainties about how even perfectly fabricated nanoscale mechanical devices should behave due to our incomplete theoretical understanding.

At sufficiently small sizes the fact that materials are comprised of atoms and are not continuous media becomes important. That size scale is quite close to atomic dimensions. Somewhat larger nanoscale structures may be described by continuum mechanics provided the theory is suitably extended to account for the occurrence of effects irrelevant in larger structures.[1] One class of these effects is related to surfaces. Since the surface area to volume ratio grows as the size of a structure is decreased, surfaces are expected to play a more prominent role at the nanoscale.

Of the various mechanical properties, the Young's modulus is of particular interest as an important parameter in the function of nanoscale devices such as flexural-mode mechanical resonators[2] and as an archetype in

terms of the scaling behavior of a variety of mechanical properties including the Poisson ratio, the anelastic damping coefficients and so on. The Young's modulus is defined as the ratio of the stress applied to stretch a cylindrical (or prismatic) beam to the resulting elongation strain. For bulk materials it may be expressed in terms of the bulk elastic constants C_{ijkl} and it is a material constant, independent of the size of the structure. If the system is comparable in size to any mechanical inhomogeneities it contains, such as grains or inclusions, the the modulus may exhibit a size dependence; interestingly, at the nanoscale even a system free from internal inhomogeneities has been predicted to have a size-dependent Young's modulus.[9,10]

Here we present in detail the results of an *ab-initio* study of the mechanical properties of silicon nanowires. Our goal is to calculate these properties from first principles, using a quantum-mechanical description of the electronic binding that is free from any empirical input or other *a priori* assumptions about the nature of the bonds. We then compare the results to existing nanomechanical models of the size dependence of the properties of nanosystems. This comparison requires the calculation of structural and mechanical properties of various reference systems, which we also report here. Some of the nanowire results have been presented previously in a more concise form.[11]

While our principal focus is on the Young's modulus, we also calculate and analyze the residual stress and equilibrium elongation of the nanowires. We consider prismatic Si [001] nanowires with a combination of {100} and {110} hydrogen-passivated surfaces, and single crystal cores as in experiment.[2,12] We have chosen the [001] orientation for the longitudinal axis because of its relevance to the NEMS devices;[2] Si nanowires grown rather than etched typically have different orientations.[13] Hydrogen passivation results from rinsing the oxidized Si surfaces with HF. It provides a standard system suitable

for a systematic study of the size dependence in nanomechanics. With other surface conditions the band gap can vary greatly, and nanowires can go from semiconducting to metallic;[14] whereas the H-passivated wires remain semiconducting[15] down to the smallest sizes studied here and the surfaces do not change the nature of Si-Si chemical bonding from its covalent character.

The article is organized as follows. We begin with a review in Section II of the state of our current understanding of the mechanics of nanoscale structures focusing on nanowires, especially nanowires composed of Group IV elements. Then we report in Section III the result of calculations of Si bulk and surface systems that are used later in the analysis of Si nanowire mechanical properties. In Section IV we describe the geometry and configuration of the nanowires studied here. We describe how the series of wires of various sizes was created, and note subtleties in the description of the wires with continuum quantities. In Section V we present and analyze the residual stress of the nanowires constrained from longitudinal relaxation. We analyze this stress and the related property of the equilibrium length of the wire. Finally, we report the result of calculation of the Young's modulus, and analyze the size dependence. The basic calculations of the Young's modulus, the residual stress and the equilibrium length were reported briefly in Ref. 11. Here we present the results for the reference systems and the detailed analysis of the mechanics not included in the short article. This analysis goes beyond the successful comparison of the first-principles results with the scaling laws derived from continuum mechanics models including surface effects presented previously[11] and allows the determination of the specific physical structures and interactions at the atomic and electronic level that lead to the size dependence. Many, but not all, of these structures and interactions are present in the surfaces of the slab reference systems that may be analyzed at much less computational cost than the nanowires. The first-principles calculations allow us to assess in detail the validity and point of breakdown of the continuum models and the physics captured therein.

II. A BRIEF REVIEW OF NANOMECHANICS

The mechanical properties of nanowires are expected to depend on the size (diameter) of the wire because surface effects increasingly dominate as the devices are miniaturized down to the nanoscale. This expectation has been borne out by computer simulation using atomistic techniques based on empirical potentials. The first such calculations were done for single-crystal α-quartz beams, finding a systematic size dependence in which the Young's modulus decreased with decreasing size.[9,10] These and calculations of the Young's modulus for various other materials have predicted a size-dependent modulus with an additive correction to the bulk value that scales like the surface area to volume ratio.[16,17]

Continuum-based formalisms for nanoscale mechanics have been proposed that include the effect of surface properties on the mechanical behavior. One class of models is based on the surface free energy and its first two strain derivatives (the surface stress and the surface elastic constants).[17–19] Other approaches make use of the Cauchy-Born rule applied to surfaces to avoid the need for precalculated surface properties for metals[20] and a Kirchoff rod model for the properties of torqued amorphous nanowires.[21] Beyond the inclusion of surface properties, there have been efforts to explore the relevance of other sources of size-dependence. A few studies claim an additional contribution that scales like the edge to volume ratio (cf. Ref. 9): such a contribution, with a factor of the logarithm of the separation of the edges, has been discussed for epitaxial quantum dots.[22–24] Another study proposes the size dependence of the Young's modulus due to the anharmonicity (nonlinearity) of the bulk elastic moduli together with the strain resulting from the surface stress.[25]

An intuitive way of understanding these effects is that there is a layer of material at the surface (and edges) whose mechanical properties differ from those of the bulk including different elastic moduli and eigenstrains. The term eigenstrain here means that the surface layer is constrained by its interface to the bulk to be at a nonzero strain with respect to its minimal energy state; i.e., at a nonequilibrium lattice constant if the surface layer is crystalline. The surface layer could be chemically distinct from the bulk, such as an oxide layer or a hydrogen-passivated surface, but the effect may be entirely due to the structural difference at the surface, such as a bare reconstructed surface. These surface effects could possibly force the system to deviate significantly from the bulk equilibrium, and go out of the linear elastic regime. Atomistic calculations provide insight into these effects, but then we must assess to what extent the results from empirical potentials can be trusted. For many multicomponent systems, empirical potentials are either not available or not validated. Even for pure Si nanowires, there is physics missing from empirical potentials that may be crucial, possibly to be included in the future in generalized potentials such as done recently for platinum nanoparticles.[26] One example is the buckled dimer reconstruction on the Si {100} surface that is not the ground state of any of the standard Si empirical potentials,[27] or even a tight-binding model.[28]

To date, experimental data on the size dependence of nanostructure mechanics are very limited. If fabricating the nanoscale structures and measuring their mechanical properties such as the Young's modulus is difficult, then the difficulty is compounded in obtaining reproducible measurements free from systematic error across a series of structures of decreasing size. Promising work has begun in this direction. Atomic force microscopy (AFM) measurements of the Young's modulus[29] (E) of cast metallic nanowires with diameters in the range of 30 to 250 nm show a strong size dependence.[30] Recent experiments

TABLE I: Bulk elastic properties calculated with DFT. The Young's modulus (E) and the Poisson's ratio (ν) have been derived from the elastic moduli C_{11} and C_{12}. All units are in GPa except for Poisson's ratio, which is dimensionless.

	This work	Other theory[42]	Experiments[50]
C_{11}	154.6	154	167.7
C_{12}	58.1	55	65.0
C_{44}	74.4	-	80.4
E_{bulk}	122.8	125.1	131.4
ν_{bulk}	0.27	0.26	0.28

have also found a strong size dependence for E of ZnO nanowires with diameters in the range of 17 to 550 nm.[31]

For semiconductor wires, Measurements of the Young's modulus and the bending modulus of crystalline boron nanowires with diameters of 40–58 nm and 43–95 nm, respectively, have shown no systematic size dependence.[32] The Young's modulus of single crystal germanium nanowires with the diameters of 40–160 nm is also found to be comparable to the bulk value.[33] A study using a different AFM technique reported a value of E of 18 ± 2 GPa for irregularly shaped < 10-nm Si $\langle 100 \rangle$ nanowires;[34] for Si$\langle 111 \rangle$ wires with 100–200 nm in diameter, E has been found to be consistent with the bulk value;[35] Si $\langle 110 \rangle$ nanowires with diameters of 12–170 nm show size-dependent softening.[36] In another Group-IV system, measurements of E for silica nanobeams have demonstrated that the way in which the beam is clamped (i.e., the boundary conditions) affects the apparent value.[37] Experimental challenges measuring the intrinsic nanoscale Young's modulus make this a topic of continued activity, leveraging earlier work on the mechanics of nanotubes.[38]

In the absence of definitive experimental data, first-principles quantum mechanical calculations based on density functional theory (DFT) can provide a robust prediction for the behavior of the nanoscale structures, but there have been few results reported. True first-principles techniques do not rely on any empirical data, solving the quantum-mechanical Kohn-Sham equations of DFT to achieve predictions from first principles.[39] One quantum study based on an empirical tight-binding technique has been published.[28,40] Recently the size dependence of the Young's modulus of thin slabs has been reported calculated from first-principles,[41,42] results that are quite relevant but not equivalent to nanowire calculations due to the absence of edges. We are not aware of any *ab initio* calculations of nanowire moduli in the literature apart from the brief article, Ref. 11.

III. BULK AND SURFACE REFERENCE CALCULATIONS

Nanowires have structural aspects ranging from bulk-like atomic arrangement in the core of wires to the more open, and often significantly relaxed, surface and edge structures. As the size of the wire decreases, the surfaces and edges play an increasing role. In this section we establish the reference properties of the bulk silicon and the surfaces needed to analyze the mechanics of hydrogen-passivated Si $\langle 001 \rangle$ wires. The reference data will help us understand the complex mechanics of nanowires in terms of simpler physics and assess how continuum surface physics parameterized by the properties of the reference systems can augment bulk continuum mechanics to provide a robust description of nanometer-scale structures.

A. Bulk properties

A series of calculations has been done to obtain the bulk properties of crystalline silicon. The history of density functional theory investigations of silicon is long, going as far back as the late 1970's.[43] The elastic constants of silicon were calculated from first principles in the work by Nielsen and Martin,[44] and anharmonic effects in silicon have been mentioned in the early work by Ihm and coworkers.[45] Our purpose in performing similar calculations in the context of this study is to provide an assessment of accuracy of our results compared to literature values, and to provide reference numbers calculated using the same code and techniques as in the nanowire calculations in order to provide directly comparable numbers to analyze the nanowire results.

We use first-principles density functional theory (DFT): specifically, the Vienna ab-initio simulation package (VASP) using the projector augmented-wave method (PAW)[46,47] within the generalized gradient approximation (GGA) by Perdew and coworkers.[48] The PAW potentials with 4 valence electrons ($3s^2 3p^2$) are used. The energy cutoff for the plane-wave expansion is 29.34 Ry, and $12 \times 12 \times 12$ Monkhorst-Pack mesh[49] is used for k-point sampling. The system consists of the 8 atoms of a single Si diamond cubic unit cell with periodic boundary conditions. The supercell is deformed to the appropriate strain and the atomic positions are fully relaxed for each calculation.

From the bulk crystal under uniaxial loading, i.e., stressed along the [001] direction and stress-free in two transverse directions, the Young's modulus and Poisson's ratio of the bulk reference system have been obtained. The equilibrium Young's modulus calculated from derivatives of a fit of the total energy in the strain range from 5% compression to 5% tension is 122.5 GPa using a fifth-order polynomial fit, the corresponding Poisson's ratio is 0.27. The value does not change significantly for a lower order fit. The difference between the second order fit and the fifth order fit is less than 1%. The negligible modulus difference between harmonic approximation and anharmonic expansion implies that the effect of bulk anharmonicity on the Young's modulus is small at these strains. Another way to assess the effect of anharmonic-
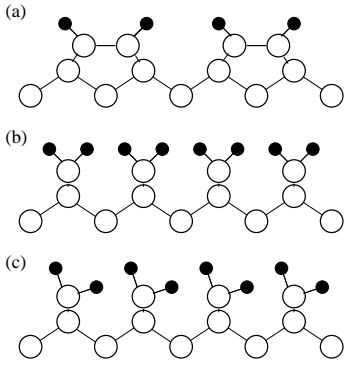
FIG. 1: Hydrogen passivation on Si(100) surface. (a) 2×1 monohydride, (b) 1×1 symmetric dihydride, and (c) 1×1 canted dihydride.
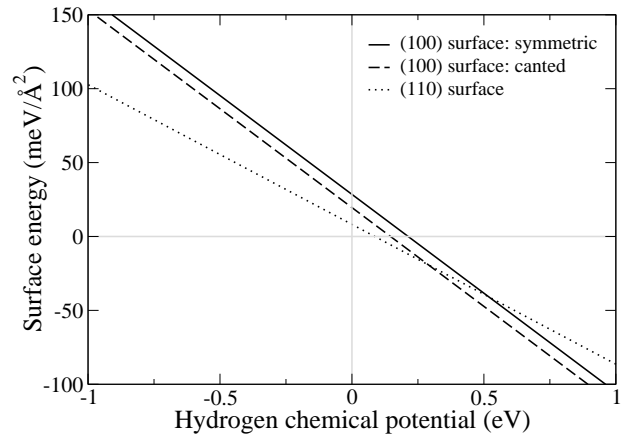

FIG. 2: Surface energies of the symmetric and canted H-terminated Si(100) surface and the H-terminated Si(110) surface as a function of hydrogen chemical potential as calculated in DFT. The hydrogen chemical potential is calculated relative to molecular hydrogen dissociation energy.

ity is to examine the compression-tension asymmetry of the modulus using the fifth order fit: 5% tension in the [001] direction results in mere 3% anharmonic increase in the Young's modulus. It is well known that the covalently bonded silicon has a weak anharmonicity compared to metals, as typically expressed in terms of a relatively small Grüneisen parameter.[51] We show below based on these reference calculations that the anharmonicity does not play an important role in the size dependence of the Young's modulus for silicon nanowires, but the conclusion might have been different in a more strongly anharmonic system.[25]

We have also computed C_{11}, C_{12} and C_{44} from separate calculations. The values we obtain are $C_{11}=154.6$ GPa, $C_{12}=58.1$ GPa and $C_{44}=74.4$ GPa, in good agreement with the previous DFT calculations, and are ∼10% less than the corresponding experimental values.[50] The Young's modulus and Poisson's ratio have been alternatively obtained from C_{11} and C_{12}, and listed in Table I. The direct numbers from strictly uniaxial stress, and indirect numbers from cubic elastic constants are essentially identical.

B. Surface properties

We now turn to the properties of the H-terminated Si surfaces so important to the nanowire mechanics. The ground states of low-index Si surfaces have long been studied both for bare (clean) reconstructed surfaces[52–54] and for hydrogen-passivated surfaces.[55,56] In recent years, after the ground states had been identified, the attention has switched to the mechanical properties of the bare surfaces for the application to Si nanowires using empirical potentials,[17] and to Si thin slabs using first principles calculations.[42] Despite considerable attention to Si surfaces, the mechanics of hydrogen-passivated surfaces has not been studied in detail.

The mechanics of the hydrogen-passivated surfaces, together with the mechanics of the bare surfaces, give an indication of the range in which the surface mechanics in the real world resides. The two surface conditions represent two opposing ideals, i.e., perfect passivation of very reactive bonds and no passivation of such dangling bonds. This idealization motivates the need to understand the mechanics of the hydrogen-passivated surfaces qualitatively as well as quantitatively as a basis for further study of the mechanics of nanowires, not to mention many other NEMS devices. In principle, the hydrogen-passivated surfaces still have a surface effect, similar to those from the bare wires, that arises from having a free surface. This is an intrinsic effect. In addition, they have another effect due to the surface hydrogen atoms, an extrinsic effect. The surfactant-induced stress has been explained within the context of local electronic environment for semiconductor surfaces,[57,58] but it is primarily due to the interaction between adsorbate and substrate atoms. Hence, it is less important for hydrogenated Si surfaces, where the hydrogen-hydrogen interaction is prominent as evidenced in the surface (ground-state) structures.[56,59] The efforts to understand the surface mechanics using experimental[60] and simulated[61] nanoindentation provide qualitative descriptions but the accurate (size-dependent) Young's modulus or the surface elastic constants have proved difficult to access via this indirect technique, leading to a need for direct measurement. In the work presented here first-principles calculations are crucial to deal properly with quantum mechanical effects such as the hydrogen-hydrogen interaction, and to investigate directly the size-dependent mechanical properties of the hydrogenated surface in a quantitative sense.

Thus, we investigate on the surface properties of the low-index facets relevant to ⟨001⟩ nanowires, Si {100} and {110} surfaces. A few surface patterns are known for the hydrogen-passivated {100} surface[56] and illustrated in Fig. 1; we have focused on the 1×1 dihydride phase partially because some of the wires in the range of interest

TABLE II: Surface energies, stresses, and elastic constants for Si {100} surface with symmetric and canted dihydride phases, and Si {110} surface calculated with DFT. For surface elastic constants, [001] is taken to be the principal direction for S_{11}, and the other in-plane direction orthogonal to [001] is taken to be the second direction for S_{22}. The surface modulus, S, is analogous to the bulk modulus, and defined as $S = (S_{11} + S_{22} + 2S_{12})/4$ when isotropic strain is applied, i.e., $\epsilon_{11} = \epsilon_{22}$.

	surface energy (meV/Å^2)	surface stress (meV/Å^2)	surface elastic constants (eV/Å^2)			
			S_{11}	S_{22}	S_{12}	S
{100} symmetric	28.5	-123.2	-1.191	-1.191	1.919	0.364
{100} canted	19.6	-55.0	-0.659	-0.659	0.457	-0.101
{110}	8.2	-1.3	-1.223	0.354	-0.614	-0.526

may be too small to develop any larger pattern fully, and partially because our focus in this work is on size effects, and thus we must have the same pattern for all sizes. It is also known that the dihydride phase is preferred over the monohydride phase at low temperature.[62]

The surface energies of hydrogenated Si surfaces we calculated in DFT are shown in Fig. 2, with the three curves corresponding to the {100} symmetric dihydride surface, the {100} canted dihydride surface, and the {110} surface. Again VASP was used, with 29.34 Ry cutoff energy and 12×12×1 Monkhorst-Pack mesh in the two-dimensional Brillouin zone. The calculations were performed on slabs with 14 layers of Si for the {100} slabs and 15 layers for the {110} slabs with a single unit cell in plane, for a total of 14 Si and 4 H atoms, and 30 Si and 4 H atoms, respectively. The atomic positions were relaxed until the force on each atom was less than 10^{-2} eV/Å.

The surface energies depend on the chemical potential of hydrogen,[56] and the hydrogen chemical potential is taken relative to the hydrogen molecule dissociation energy; i.e., zero chemical potential implies that the hydrogens dissociate from the molecule and attach to the surface to terminate the dangling bonds without any cost in energy. The zero-point-energy term[56] is omitted, but this term only shifts the energy and does not alter the physics. The choice of the reference chemical potential is somewhat arbitrary but this choice measuring the chemical potential relative to the H_2 dissociation energy facilitates comparison of the two {100} surfaces: a change in the hydrogen chemical potential adds the same offset to both surface energies, and only the surface energy difference matters. The horizontal line represents zero surface energy, and below this line the surface energy is negative; i.e., surface area is maximized at the cost of material cohesion. We are interested in the region above the zero-surface-energy line, and we find that the {110} surface is preferred over the other two surfaces.

The surface stress can be unambiguously determined since it is a strain derivative of the surface energy, and hence the chemical potential dependence goes away. The surface stress has been calculated for various materials previously using first-principles[63] and classical atomistic[64] techniques. As can be seen in Table II, the surface stress is twice larger for the symmetric {100} surface stress than for the canted {100} surface. The strong

H-H repulsion between neighboring hydrogen atoms is relaxed by tilting the dihydride, and the surface stress is reduced. The negative stress indicates compression. The surface stress of the {110} surface is essentially negligible. Across a range of loading conditions and fitting procedures, its values are small, varying little and what variation there is most likely comes from a numerical artifact: the surface stress under [001] strain ranges from -1.3 to -3.2 meV/Å^2 depending on the order of fitting. The resulting uncertainty due to the fitting in the equilibrium surface lattice spacing is less than 10^{-3} Å for the 15-layer {110} slab.

The next derivative (second strain derivative) of the surface energy is the surface elastic constant. Similar to bulk elastic constants, surface elastic constants account for the material stiffness. Three surface elastic constants, S_{11}, S_{22} and S_{12} have been calculated with the principal direction of [001]. The negative constants indicate softening due to the surface, and the opposite signs of S_{11} and S_{12} can be thought of as a negative Poisson effect. For example, a higher positive S_{12} for the symmetric {100} surface means that, when the surface slab is stretched in the [001] direction, the slab would expand (direction of energy reduction) in the transverse direction as well due to the particular alignment of the dihydride in the [110] direction. On the other hand, a positive Poisson effect has been observed for the {110} slab. This conventional result is expected as there is virtually no H-H repulsion on that facet.

Also presented is the surface modulus, S, a two dimensional counterpart of the bulk modulus under hydrostatic loading. As expected, the {100} symmetric surface has the highest surface modulus, the {100} canted surface is next, and the {110} surface shows the lowest modulus: the hydrogen repulsion is highest for the {100} symmetric surface, and it is virtually zero for the {110} surface. The strong repulsion of the symmetric dihydride even leads to a positive surface modulus, implying that, in the case of isotropic plane stress the {100} symmetric surface slab is even stiffer than the bulk system with the same volume. However, the increase in individual elastic constants shows a different tendency than that of the surface moduli: the S_{11} is highest for the {100} canted surface. We believe that this may be explained by the relaxation of the hydrogen repulsion during uniaxial strain. The uniaxial strain in the [001] direction induces the shear

strain for the {100} surface unit cell, and dihydrides become misaligned and consequently the associated repulsion is more or less relaxed. In this situation, the H-H repulsion may be substantially relaxed with respect to the applied strain for the {100} canted surface. On the other hand, {100} symmetric surface seems to undergo a smaller change in the H-H interaction energy and its contribution to S_{11} is also smaller. Again, this change has nothing to do with the absolute magnitude of hydrogen interaction. Rather, the magnitude of modulus is directly related to the interaction energy change with respect to the given strain, in particular the curvature with respect to the applied strain.

To summarize, the stiffening effect of the surface hydrogen for the {100} canted surface is equally noticeable under uniaxial and biaxial strain, but the effect seems prominent under biaxial strain for the {100} symmetric surface. In other words, an arbitrary strain would relieve the hydrogen repulsion for the {100} canted surface, but a uniform biaxial strain would dominantly do it for the {100} symmetric surface. This complexity of the hydrogenated {100} surface comes from the fact that the principal crystallographic directions of the bulk are $\langle 001 \rangle$ directions, whereas those of the {100} dihydride surface are $\langle 110 \rangle$ directions: the principal directions from one perspective are the maximum shear directions from the other.

The two hydrogenated {100} surfaces, symmetric and canted, have substantial differences in their surface stress and surface moduli, and the resulting equilibrium surface lattice spacings for the 14-layer slab ($\sim$1.96 nm thick) are 1.83% and 0.76% longer than the bulk lattice, respectively. The 15-layer {110} slab ($\sim$2.95 nm thick) exhibits the elongation on the order of 0.01%, i.e., less than 10^{-3} Å difference from the bulk spacing, due to its negligible intrinsic surface stress.

C. Silane chains

In order to separate the hydrogen interatomic (H-H) interaction contribution from the other contributions to the surface elastic constants, the effect of surface hydrogen is evaluated from a periodic chain of silane molecules, in which the dominant H-H repulsive interaction is coming from neighboring silane molecules. The periodic chain is taken from the fully relaxed {100} surface slab as illustrated in Fig. 3, and the backbonds are terminated with 2 additional hydrogen atoms. The bond angles of the relaxed slab geometry are preserved, and the backbond length is chosen to be 1.49 Å based on the structure of an isolated SiH$_4$ molecule. The canted silane chain is shown, but the same procedure is applied to the symmetric chain. The extrinsic contribution to the surface elastic constants from the H-H interaction is given approximately by

$$S_{11}^{H-H} = \frac{1-\nu}{\sqrt{2}A} \partial^2 U^{H-H} / \partial \epsilon_{zz}^2 \Big|_0 \qquad (1)$$
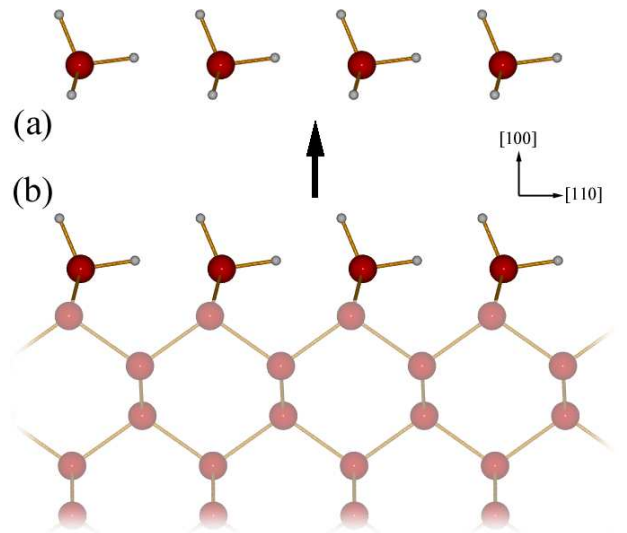

FIG. 3: (Color online) One dimensional periodic chain of silanes and its relationship to the (100) surface. The silane chain, (a), has been taken from the fully-relaxed hydrogenated (100) surface with canted dihydrides, (b), and the backbonds have been passivated with additional hydrogens.
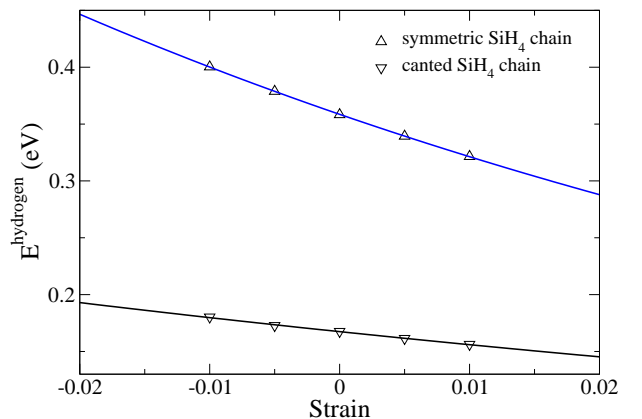

FIG. 4: (Color online) SiH$_4$-SiH$_4$ interaction energy calculated in DFT as a function of strain for the symmetric and canted chains. The solid curve is an exponential fit to the presented data.

where U^{H-H} is the H-H contribution to the total energy and A the area covered by one silane. The prefactor is due to the decomposition into the longitudinal and transverse directions of the wire including the Poisson effect with $\nu \approx \nu_{bulk} = 0.27$. U^{H-H} can be approximated by the silane-silane interaction energy in the chain and given as

$$U^{H-H}(\epsilon) \approx U^{chain}[N, \epsilon]/N - U^{silane} \qquad (2)$$

where $U^{chain}[N]$ is the total energy of the N-molecule chain of SiH$_4$, and U^{silane} is the energy of a single SiH$_4$ molecule. U^{H-H} can be interpreted as a energy penalty to bring repulsive silane molecules into a single chain.

It is a reasonable approximation in the sense that the underlying physics is essentially identical in both cases: H-H exchange repulsion is the dominant interaction, and both the SiH$_2$ group on the {100} surface and SiH$_4$ in the silane chain have almost identical local environments.

U^{H-H} as a function of strain is obtained from a series of silane chains, whose geometries are taken from the corresponding relaxed {100} surface slabs. Due to the nature of H-H repulsion, U^{H-H} is fitted to an exponential function around the bulk lattice spacing as shown in Fig. 4. The fit of an exponential form to the data yielded the following dependence:

$$U^{H-H}_{\text{symmetric}} = 0.359 \ \exp(-10.97\epsilon) \qquad (3)$$
$$U^{H-H}_{\text{canted}} = 0.167 \ \exp(-7.10\epsilon) \qquad (4)$$

in units of eV. The ideal S^{H-H}_{11} obtained from the silane chains using Eq. 1 for the symmetric {100} and canted {100} slabs are 1.488 eV/Å^2 and 0.291 eV/Å^2, respectively.

IV. GEOMETRY OF NANOWIRES

The cross-sectional shape of the Si $\langle 001 \rangle$ wires we study is a truncated square with four {100} facets and four {110} facets. Some wires studied here have no {100} facets; for those that do, the ratio of the facet areas is taken to be roughly in accordance with the Wulff shape for a bare wire with {100}-p(2×2) and {110}-(1×1) surface reconstructions; i.e., the ratio of {100} to {110} area is 3.5:1.

The reason for using the Wulff shape of bare nanowires is that the effect of surface condition on the material stiffness can be addressed by comparing hydrogen passivated wires and bare wires. In the Wulff shape of hydrogen-passivated wires, the {110} area would be larger than the {100} area due to the lower energy of that facet, opposite to the Wulff shape of bare nanowires used here. It is advantageous to use the bare-wire shape not only because the surface energy of a bare slab can be unambiguously determined whereas that of a slab with surface adsorbates such as hydrogen depends on the adsorbate chemical potential, but because having a common cross section allows us to focus on the size effect or the role of surface condition apart from any effect due to shape. The detailed comparison of the bare and H-terminated wires will be given elsewhere.[65]

The electronic structure of nanowires is one dimensional. It requires a large electronic excitation to probe the transverse dimensions of the wire. The mechanics of the nanowire, while not fully three dimensional, has unavoidable three dimensional aspects to it. The nanowires have a finite cross-sectional area that enters into many of their mechanical properties and because of this cross section they are able to support mechanical bending moments. The relevance of the transverse dimensions to
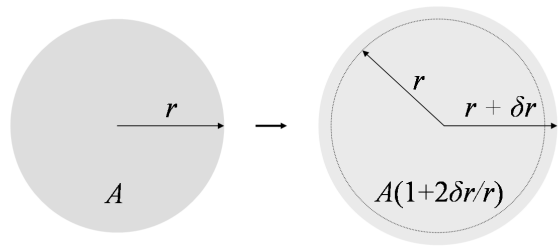

FIG. 5: Size effect of the definition of the cross-sectional area. The dotted circle in the second circle indicates the initial size whose cross-sectional area is A.

mechanical properties poses a challenge. The mechanical properties are most succinctly phrased in terms of continuum mechanics, but this requires the definition of continuum measures such as the cross-sectional area and the transverse dimensions in terms of atomistic properties such as ionic positions or electron densities.

To calculate the Young's modulus, for example, *we define the cross-sectional area to be the area bounded by the centers of the outermost (H) atoms.* This choice is motivated by the fact that the volume excluded by the beam from access by outside atoms is determined from the forces arising from electron interactions. In other words, any experimental measure of volume is based on the probe being strongly repelled due to electron interactions rather than between those of nuclei. Therefore, a system that can be thought of as a discrete system in an atomic description is continuous in an electronic description. It is unusual, however, to apply the techniques of continuum mechanics at subatomic length scales,[66] and indeed conventional scale-free continuum mechanics breaks down at nanometer scales or higher because of the lack of physics relevant to small structures such as surface energies and surface stresses.

The surface definition used here ensures that most of the electron density is enclosed by the surface, the boundary formed by H atoms, and the electron density from Si atoms essentially vanishes beyond this point. In addition, the positions of the nuclei are well defined and not subjective. Other definitions of the bounding surface exist: for example, the midplane between two identical H-passivated surfaces at their minimum energy separation.[59]

Had we taken a different definition of the cross-sectional area, the apparent size dependence of E would have been different, an ambiguity associated with describing discrete atomic systems with continuum mechanics. To illustrate the issue, consider the effect on the size dependence of E from changing the definition of cross-sectional area by modifying the position of the surface r by δr as shown in Fig. 5; e.g. δr would be the atomic radius for a surface going through atomic centers vs. one circumscribing their electron cloud. The change δr takes

A to $A' \approx A(1 + 2\delta r/r)$

$$E(r) \;=\; \frac{F}{A\epsilon} \tag{5}$$

$$E'(r) \;=\; \frac{F}{A'\epsilon} \tag{6}$$

$$\approx \; \frac{F}{A\,(1 + 2\delta r/r)\,\epsilon} \tag{7}$$

$$= \; E\,(1 - 2\delta r/r + \cdots) \tag{8}$$

where F is the force carried by the beam and ϵ is the resulting strain. The leading change to the Young's modulus, $-2E(\infty)\,\delta r/r$, is proportional to the surface area to volume ratio. This change modifies the value coefficient of the surface-area-to-volume ratio term in the Young's modulus, so when we calculate this coefficient, it is implicit that its value is with respect to our prescription for the location of the surface. The uncertainty vanishes as the system size is increased, i.e., the surface to volume ratio is decreased, and this level of ambiguity is completely negligible for the modulus of macro-scale structures.

V. NANOWIRE CALCULATIONS

For each of the nanowire geometries shown in Fig. 6, the Si atoms were initially positioned at their bulk lattice sites and hydrogen atoms were added to terminate the bonds at the surfaces, and this configuration was relaxed. The surface structure, such as the ground state canted dihydride {100} surface, is obtained naturally from the relaxation and requires no initial seeding. The supercell size of each wire is one cubic unit cell long along the wire, and has more than 10 Å vacuum space in the transverse directions. The numbers of Si atoms and H atoms in the supercell for each of the geometries are also shown in Fig. 6.

Again the first-principles DFT code VASP has been used for the calculations, as described above. The energy cutoff for the plane-wave expansion is 29.34 Ry, and $1{\times}1{\times}12$ Monkhorst-Pack mesh,[49] or six points in the one dimensional irreducible Brillouin zone, is used for k-point sampling. The relaxation convergence criterion was that the force on each atom be smaller than 2×10^{-3} eV/Å for the 1.49-nm and smaller wires, and 10^{-2} eV/Å for the larger wires, for which convergence of the Young's modulus was attained with the less stringent tolerance. The residual stress, equilibrium length and Young's modulus have been calculated for the range of wire sizes shown in Fig. 6.

The extent of the range of wire sizes is dictated by computer resource limitations. The calculations for the largest wire, the 3.92-nm wire, required roughly 922 hours using typically 128 processors on the 2.3 GHz Xeon-based MCR supercomputer, for a total of 109 285 CPU-hours for this one wire. For the final stages of the relaxation, in which the calculation setup as described above was applied, it was necessary to use up to 512 processors.

A. Residual stress

Residual stress can be a problem or a feature of doubly clamped oscillators. During etching in the device fabrication process, stress forms in the mechanical structure. This stress shifts the resonant frequency of the mechanical beam, and it can affect other properties such as dissipation. For example, recently resonators with very high quality factors have been demonstrated at room temperature using silicon nitride nanobeams under high tensile stress.[67] Residual stress may arise due to a number of physical phenomena. One example is the residual stress coming from surface stress due to interactions in the passivation layer, and it is this effect in the H-passivated Si nanowires that we investigate now. Within our DFT calculations, the residual stress is equated to the axial stress when the longitudinal wire lattice spacing is fixed at the bulk value, $\sigma_{zz}(L_0)$.

To calculate the residual stress, the system was initially relaxed to its zero-temperature minimum energy with the length of the periodic supercell held fixed at the bulk lattice spacing in the longitudinal direction. Then the relaxed total energy was calculated for each beam in a series of longitudinal strains at increments of roughly 0.5%. These total energy values were fit to a polynomial.

We then obtain the residual stress and other important properties from the strain derivatives of the polynomial: the first derivative gives the axial stress, σ_{zz}, the minimum of the polynomial, ϵ_{zz-eq}, gives the strain corresponding to the equilibrium length, and the value of the curvature at the minimum gives the Young's modulus E:

$$\sigma_{zz}(\epsilon_{zz}) \;=\; V^{-1}\partial U/\partial\epsilon_{zz} \tag{9}$$

$$\sigma_{zz}(\epsilon_{zz-eq}) \;=\; 0 \tag{10}$$

$$E \;=\; V^{-1}\partial^2 U/\partial\epsilon_{zz}^2\big|_{\epsilon_{zz-eq}} \tag{11}$$

where U is the DFT total energy. The equilibrium length L_{eq} is determined from the equilibrium strain and the initial length L_0 according to

$$L_{eq} = L_0\,(1 + \epsilon_{zz-eq}) \tag{12}$$

where here and throughout the article we are using engineering strain, which is adequate for the small strains of interest. The details of the equilibrium length and the Young's modulus are discussed in the next two subsections. We focus on the stress in this subsection.

The size dependence of the residual stress of the H passivated Si nanowires evident in Fig. 7 is driven by compressive surface stress. The residual stress may be decomposed into core and surface contributions. The latter may be further decomposed into extrinsic surface contributions from hydrogen (H-H) interactions and intrinsic surface contributions from the change to the Si bonds near the surface compared to the Si bulk (Si-H and modified bond order Si-Si). Since DFT only provides a total energy, this decomposition is somewhat ambiguous. Techniques such as Bond Order Potentials[68]
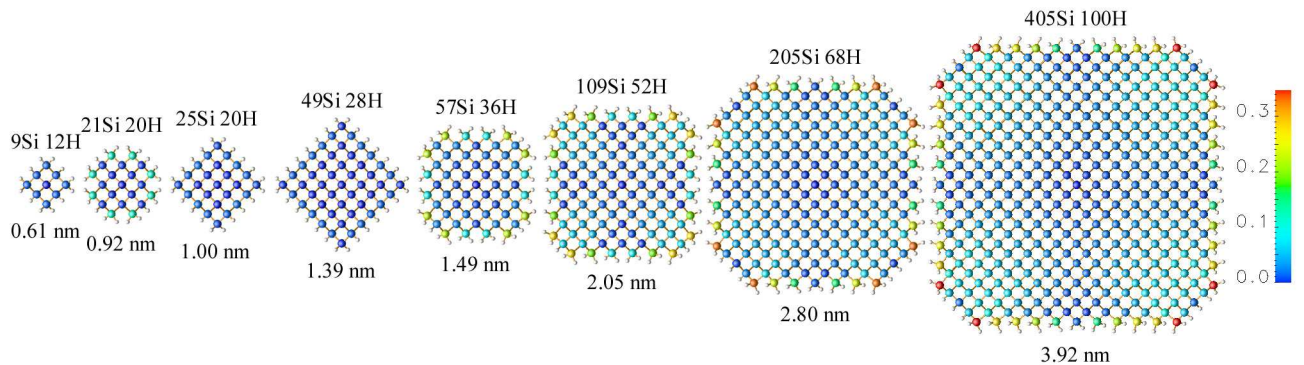
FIG. 6: (Color online) Cross sections of fully relaxed hydrogen-passivated wires, with each Si atoms colored as shown in the legend corresponding to its transverse relaxation in Å. The numbers above the wires stand for the number of atoms in the supercell. For example, 405Si 100H means that the supercell has 405 Si atoms and 100 H atoms. The numbers below represent the wire width, where the width is defined as the square root of the cross-sectional area.

and the Generalized Pseudopotential Theory[69] have been introduced as formalisms for extracting atomic interactions from the underlying quantum mechanics. They are not sufficiently developed to apply to nanowires, however. Local moment techniques also provide a partition of the total energy atom by atom, but they too are insufficiently accurate for our purposes. Instead, we separate different contributions to the nanowire properties through the use of reference systems. In the first instance, the continuum models require core and surface properties: the uniformly strained bulk Si systems of Section III A provide an approximation to the core of the nanowire and the slab surface calculations of Section III B give an approximation to the nanowire surfaces. In a more refined analysis we decompose the surface contribution further and estimate the extrinsic surface (H-H) interactions to be equal to those of neighboring hydrogens in two silane molecules in the orientation and separation of the H-passivated surface. The intrinsic contribution is the remainder, i.e., the part that does not come from the core or the extrinsic surface interactions. The further decomposition of the surface effects into intrinsic and extrinsic enables us to begin to attribute the size dependence to specific physical processes of bonding and deformation in the surface, sub-surface and core regions of the wire.

The extrinsic contribution to the residual stress is the most important, as we now show. The intrinsic surface stress is small, as expected since the dangling Si bonds are well terminated with H atoms and the Si-Si bond order is not significantly different than in the bulk. The small magnitude of the intrinsic stress is best seen in the case of the 1.39-nm wire for which the elongation is less than 0.1% compared to ~1.5% of the 1.49-nm wire. The absence of {100} facets on this wire leads to a small extrinsic stress since the H-H separation on the {110} facets is relatively large. This smallness was already confirmed in the previous section where the surface stress of the {110} surface has been found to be negligible. The difference between these two facets is that the vacant Si

sites above the facets are filled by one and two H atoms on {110} and {100}, respectively, and the double occupancy, albeit with ~2 Å H-H separation due to the shorter Si-H bond, leads to more repulsion for {100} as discussed in Sec. II.

The extrinsic surface stress due to the H-H repulsion on the {100} facets quantitatively accounts for both the compressive residual stress $\sigma_{zz}(L_0)$ and the elongated equilibrium length L_{eq} of the nanowires. They are related to leading order through the linear elasticity:

$$\sigma_{zz}(L_0) = \sigma_{zz}(core) + \frac{1}{A}\sum_i \tau_{zz}^{(i)} w_i \quad (13)$$

$$(L_0 - L_{eq})/L_{eq} \sim \sigma_{zz}(L_0)/E \quad (14)$$

where A is the cross-sectional area, w_i is the width, $\tau_{zz}^{(i)}$ is the longitudinal surface stress of facet i, and L_0 is the bulk length of the beam. E is the Young's modulus of the beam. In principle Eq. (14) has anharmonic corrections, but the strains are small and the harmonic approximation should be good. For constant surface stress, the second term in Eq. (13) is proportional to the surface area to volume ratio; the core stress is too, since the surface stress causes a transverse expansion of the wire that induces a tensile core stress. It may be seen in Fig. 6 that surface Si atoms on the {100} facets undergo a substantial transverse expansion, where for example a 0.3 Å expansion amounts to a 13% change in the bulk Si-Si bond length. It also induces the deformation noticeable throughout the wire, extended deep into the core except for some of the high symmetry lines where the expansions toward opposite directions cancel. Hence, the transverse displacement would be hardly seen when the {100} facets are not present: the {110}-facet wires with no {100} facets, compared to those with the {100} facets, have a negligible surface expansion and the resulting in-plane deformation of the core.

The core stress arises as a kind of Laplace pressure and may be estimated through a generalized Young-Laplace
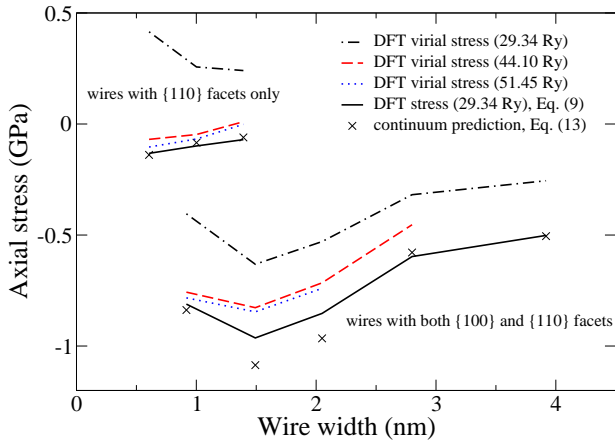
FIG. 7: (Color online) Silicon nanowire axial stress as a function of wire size calculated in DFT. The virial stresses are obtained directly from virial formula at the given cutoff energy indicated in the parenthesis, whereas the DFT stress is deduced from Eq. 9. The predictions of Eq. 13 are also plotted for which the surfaces stresses are given in Table II.
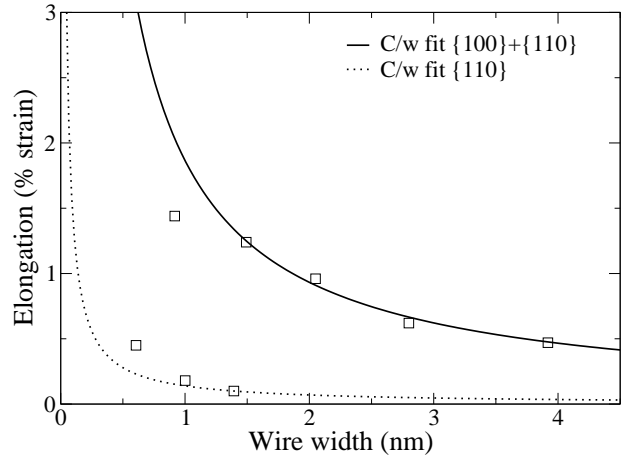

FIG. 8: Silicon nanowire equilibrium elongation strain as a function of wire size calculated in DFT. The solid curve is a fit to C/w of the elongation strain to four data points from 1.49-nm and larger wires, with $C=1.9\%$-nm. The dotted curve is a fit to C/w of the elongation strain to the 1.39-nm wire, with $C=0.14\%$-nm.

equation relating the compression of the core to the surface stress. The derivation of the expression is somewhat lengthy and presented elsewhere.[70] The result for the axial stress in the core averaged across the cross section of the wire is

$$\sigma_{zz}(core) = -\frac{8}{\pi}\nu\tau^{\{100\}}/w, \qquad (15)$$

where w is the width of the nanowire, $\nu = C_{12}/(C_{11} + C_{12})$ is the Poisson ratio and C_{11} and C_{12} are the bulk elastic constants. Here a compressive surface stress ($\tau < 0$) leads to to a tensile axial stress ($\sigma_{zz} > 0$).

The residual stress values evaluated with a few different approaches are plotted in Fig. 7. The curves denoted as 'virial' are the stresses directly obtained from the calculations via virial theorem. The stress curve denoted simply as 'DFT stress' is due to Eq. (9), and the one denoted as 'prediction' is due to Eq. (13). The virial stress evaluation is poor even for reasonably high cutoff energies, i.e., the predicted stress in some cases has the opposite sign with 29.34 Ry cutoff, and a reasonable evaluation requires a prohibitively high cutoff energy. On the other hand, the stress obtained by the strain derivative of the total energy with the same cutoff energy is less prone to the basis set incompleteness critical to the direct measure, and shows better agreement with the stress with the highest cutoff energy tested. In addition, it is advantageous as we can obtain the stress information of larger wires, where the cutoff energy is restricted due to computational cost. Considering the discrepancy between the stress due to Eq. (9) and the virial stress with the highest cutoff energy, the true stress is likely to be between the two: the convergence error for direct evaluation seems to be negative and polynomial fitting error may be positive.

For the prediction based on the bulk and surface energies, using the values from Tables I and II in Eq. (13)

gives predictions in very good agreement with the full nanowire calculations as shown in Fig. 7. The scatter for 1.49- and 2.05-nm wires may be accounted for by small edge effects. The 0.61-, 1.00- and 1.39-nm wires have no {100} facets and almost no residual stress as described above. In the case of the second smallest (0.92-nm) wire, all of the {100} atoms undergo substantial relaxation, as shown in Fig. 6, lowering the magnitude of the surface stress and the elongation. This high level of agreement gives us confidence that we understand the physics of the size dependence of the residual stress.

B. Equilibrium length

The residual stress is a direct measure of the effect of surface stress on doubly clamped nanowires. The analogous property of unconstrained (free floating or cantilever) nanowires is the equilibrium length. It is a property that is, at least in principle, directly measurable through x-ray diffraction.

The equilibrium elongation plotted in Fig. 8 shows a systematic increase in the elongation as the size of the wire is reduced, with the data falling into two series. The series are distinguished by the amount of {100} surface area, as discussed below. A solid curve representing the function C/w has been superimposed on one series of data, where w is the width of the wire. The good fit of this function, with $C = 1.9\%-$nm, demonstrates that the elongation is proportional to the surface-area-to-volume ratio. The axial stress shown in Fig. 7 exhibits a similar trend, with the stress increasing as the size of the wire decreases. Again, the deviation of the 0.92-nm wire from the curve can be explained by the reduction in the surface repulsion due to the substantial relaxation around the

edges. Equivalently, it can be explained that the wire is too small to have well defined {100} facets that would otherwise give comparable surface effects to those on the larger wires.

As is the case with the residual stress (Fig. 7), the wires in the series with elongation values closer to zero have no {100} facets. These wires show a significantly smaller amount of elongation compared to those in the series with {100} facets. The elongation for the 1.39-nm wire is less than 0.1%, and to achieve a comparably small amount of elongation in a wire with {100} facets, the wire would need to be 19 nm in width based on the above fit. The elongation would also be negligible for a larger wire with the same cross-sectional shape, as confirmed by considering that the elongation for the 2.95-nm thick {110} slab is less than 10^{-3} Å.

While the elongation of the {110}-faceted wires is considerably smaller than that of their {100}-faceted counterparts, it is actually larger than expected: as can be seen from the dotted curve in Fig. 8, the elongation of the smallest wire is even larger by roughly a factor of 2 than the C/w extension from the 1.39-nm wire, let alone any potential size-dependent effects beyond the surface effect on the 1.39-nm wire. We do not have a conclusive explanation for this enhanced size dependence. It could be due to an edge effect, but it seems more likely that it is a nonlocal surface-surface interaction effect: for these smallest wires, each facet begins to interact with opposite facet via electronic interactions. For example, the 1.00-nm wire has only 5 Si layers across its cross section. It is known from slab calculations that the effective surface properties are modified if the slab is too thin, and we expect an analogous effect here.

C. Young's modulus

We now consider the size dependence of the Young's modulus, the principal subject of this work. The Young's modulus is the second derivative of the DFT total energy with respect to the applied longitudinal strain divided by the volume (11). As a second derivative, it is the most sensitive of the quantities we compute, determining the values of the planewave cutoff, number of k points and residual force tolerance quoted above. Also, it is potentially susceptible to an unwanted dependence on the polynomial fitting procedure used for the energy. In principle, higher order fits should be more accurate, accommodating any anharmonicity but at the cost of the need for additional data (more relaxed total energy calculations). The Young's modulus of the 1.49-nm wire gives an indication of the sensitivity to the order of the polynomial fit, as described in Ref. 11. Fortunately, for the given order of fit, a higher cutoff energy does not significantly improve the fit; i.e., the largest convergence error is 0.63% for the 2nd-order fit compared to the highest order fit. We find that the second order fit with 29.34 Ry energy cutoff is reasonably good, differing by less than 2% compared with all the higher-order combinations tested, and it is the second order fit that we use for the analysis of all of the nanowires, and it permits direct comparison of the results from the entire range of nanowire sizes up to 405 Si and 100 H atoms at a tolerable computational cost. We have used this technique for a systematic study of the size dependence of the Young's modulus.

The main result is that the Young's modulus becomes softer monotonically as the size is decreased as shown in Fig. 9 and that decrease is well described by a continuum model. It drops from the bulk value ($E_{bulk}^{\mathrm{DFT}} = 122.5$ GPa) roughly in proportion to the surface area to volume ratio. It does not exhibit a strong dependence on the ratio of the {100} to {110} area seen in the equilibrium length. The smallest Young's modulus we find for any of the nanowires studied here is 29.4 GPa, the value for the smallest (0.61-nm) nanowire. This value is larger than the 18 ± 2 GPa reported from experiments on an irregularly shaped < 10-nm Si $\langle 100 \rangle$ nanowire.[34] Since the shapes are different, direct comparison is challenging, but we note that the experimental stress-strain curve is complex. Some regions of the stress-strain curve are in better agreement with the range of values we report here than the region from which the value of 18 GPa was extracted. In any case, they do report a softening of the Young's modulus as we have found in the first-principles calculations.

From continuum mechanics neglecting edge and nonlocal effects, the modulus can be expressed, slightly generalizing Ref. 17, as

$$E = E(core) + \frac{1}{A} \sum_i S^{(i)} w_i \qquad (16)$$

where $S^{(i)}$ is the surface elastic constant, a strain-derivative of the surface stress including both extrinsic and intrinsic parts. Thus, the Young's modulus may be decomposed into core and intrinsic, and extrinsic surface contributions as was done for the residual stress.

We found above that the extrinsic H-H interactions dominated the surface stress and the residual stress of the nanowires. It is less clear *a priori* what should dominate the Young's modulus, but the fact that the modulus is insensitive to the facet ratio (whether the {100} facets are present or not) suggests several conclusions:

- The core anharmonicity is irrelevant since the modulus is not correlated with the equilibrium elongation;

- The extrinsic contribution to the modulus (which is strongly facet dependent) is small;

- The intrinsic surface elastic constant dominates and its {100} value may be nearly sufficient to determine E.

Additional evidence supports each of these conclusions, as we now show.

To quantify the core contribution, we calculated that the Young's modulus of the bulk crystal increases by only 1.6% when strained ∼1.5% to match the most strained (0.92-nm) wire. This change is negligible compared to the observed softening (contrary to the finding that the bulk anharmonicity dominates the size dependence of the Young's modulus of embedded-atom-method copper nanowires[25]).

The extrinsic effect is also small, but not negligible. Based on silane interaction forces for the canted {100} surface geometry, the extrinsic contribution to the Young's modulus can be described as

$$\Delta E^{H-H} = \frac{1}{A} \sum_i S_{11}^{H-H} w_i^{\{100\}} \qquad (17)$$

where $w_i^{\{100\}}$ is the width of a {100} facet i. We have estimated that the extrinsic contribution is ∼8 GPa for the 1.49-nm wire, roughly equal to E(1.49nm)-E(1.39nm), i.e., the difference in the moduli with and without {100} facets. Here, the canted dihydride is particularly important in that the initial (unrelaxed) symmetric dihydrides on the {100} facets of nanowires relax to a configuration very similar to the canted dihydrides as illustrated in Fig. 6, only somewhat strained due to the symmetry breaking at the edges that destroys the in-plane periodicity of the infinite surface. Also, given the agreement for the residual stress and elongation between our continuum-based prediction with the canted {100} surface properties and the DFT result, we can again confirm that the canted surface is indeed relevant to the relaxed wires. Otherwise, the predicted residual stress and the elongation based on the symmetric {100} facet would be twice larger than the actual value for the 1.49-nm or larger wires.[71]

The intrinsic contribution accounts for most of the Young's modulus. By definition, it is the remainder once the core and extrinsic contributions have been subtracted, and those contributions are small as we just showed. We may go further and create a qualitative map of the intrinsic contribution using a bond-strength calculation akin to an Einstein model with independent harmonic oscillators. A small longitudinal displacement is applied to each atom, and by measuring the induced force, the spring constant for each atom is deduced. Each atom has three spatial degrees of freedom and hence three oscillators, and only the longitudinal oscillators are considered here. As can be seen in Fig. 10, surface atoms have substantially softer bonds. The true intrinsic effect might be even greater since the force built up on the neighboring atoms by displacing a single atom is relieved somewhat by the relaxation of its neighbors. The fluctuation of the spring constant for fully coordinated atoms may be explained by the electron density variation due to the surface relaxation and the natural structure of silane chains, i.e., Friedel-like oscillations. Some recent work has considered the effect of electron density variation on mechanical properties through a bond-order approach.[72]

We have also calculated the size dependence of the modulus using Eq. (16) based on the surface elastic con-
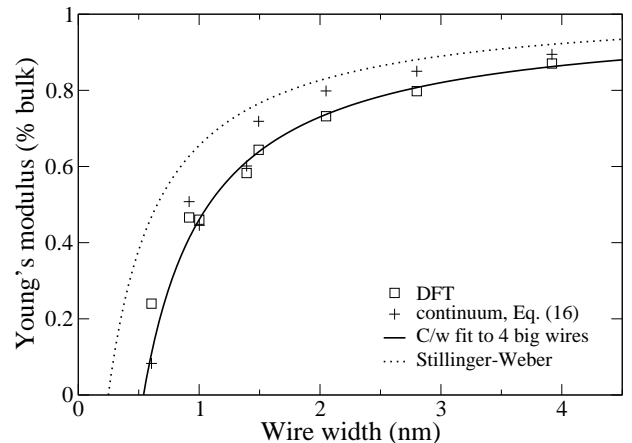

FIG. 9: Silicon nanowire Young's modulus as a function of wire size as calculated in DFT. For comparison the predictions of continuum formula (16) are also plotted, for which the surface elastic constants are obtained from the {100} canted slabs and the {110} slabs. See Section III for details. The solid curve $E = E_{bulk}^{DFT} - C/w$, with C=66.11 GPa/nm, is a best fit to a pure surface area to volume size dependence.

stants $S^{\{100\}}$ from the surface reference system presented in Table II. The results, shown in Fig. 9, are in good agreement with the full first-principles calculation, and adding the core contribution slightly improves the agreement. The reason for the scatter for 1.49- and 2.05-nm wires is two-fold. First, there is a variation in the tilting angle of the hydrides on the wire surface: those around the facet center are equal or closer to the symmetric configuration, i.e., no tilting or smaller tilting angle. The modulus estimation based only on the canted surface elastic constants could overshoot the real value. The size of the symmetric dihydride region at the middle of the facet is determined by the usual kink analysis and is essentially independent of the size of the facet. Second, the scatter for 1.49- and 2.05-nm wires may be due in part to small edge effects. Both the effect of the symmetric dihydride region and that of the edges would scale as the ratio of their constant areas to the facet area, and would therefore be less important for larger wires. Also plotted in Fig. 9 is the best fit curve of Ref. 17 from Stillinger-Weber (SW) empirical molecular statics calculations. The SW bulk Young's modulus is 13% lower and the coefficient C of the $1/w$ term is 29% lower, i.e. smaller surface effect, than the DFT values. The errors compensate for each other, leading to reasonable agreement for the nanoscale wires. This level of agreement is unexpected since the SW potential does not have the relevant nanophysics in its functional form or its fitting database and the strength of the bonds does not change at the surface. Also, the SW nanowire calculation does not include a H-terminated surface, and thus the residual stress and equilibrium elongation are quite different.
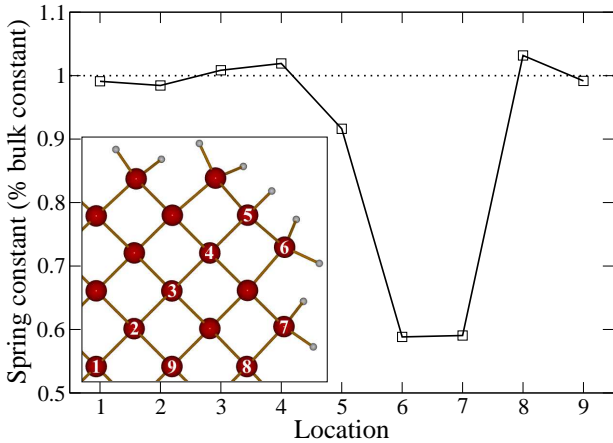
FIG. 10: (Color online) Spring constant of Si atoms for the 1.49-nm wire. The inset illustrates the location of each atom in the cross section: a quarter of the cross section is shown with the rest of the wire related by mirror symmetry, where atom 1 is located at the center of the cross-section.

VI. CONCLUSIONS

In conclusion we have found that first-principles calculation of several mechanical properties of silicon wires predicts a size dependence at the nanoscale. The form of the size dependence is in good agreement with previous models based on empirical atomistic and continuum techniques, for all but the smallest wires in which effects such as the electronic interaction between surfaces are not captured in the models. The calculations presented here enabled an analysis of the magnitude of surface and edge effects in the nanowire Young's modulus from first principles. In each case the size dependence scales roughly as the surface area to volume ratio, but for different reasons. For the equilibrium length and residual stress it is due to the extrinsic surface stress from interactions in the H passivation layer; for the Young's modulus it arises from the intrinsic contribution to the surface elastic constant. The equilibrium length and residual stress depend strongly on whether {100} facets are present or not, whereas the Young's modulus was essentially insensitive to the facet type. Surface parameters from slab calculations capture most, but not all, of the physics. The size effect is not strong for the H-terminated surfaces studied here: the Young's modulus is softened by about 50% for a 1-nm diameter wire. It may be possible to measure this effect directly using either AFM deflection or resonant frequency measurements in a double-clamped or cantilever configuration. The change in the equilibrium length is measurable with x-ray or electron diffraction techniques. These effect could be substantially stronger in silicon nanowires with different surfaces, such as bare

or oxide surfaces, making measurement easier. These systems are more challenging for first-principles calculation due to a greater number of candidate structures and a greater role for charge transfer in the mechanics. It is not clear whether the Young's modulus would increase or decrease as the size of the beam is reduced. There is much to be learned still.

In the wires we have studied the surface atoms are passivated by hydrogen atoms so that the chemical bonding is the same as in the bulk and quantum confinement is evident, the local electronic environment of each Si atom is uniform throughout the wire apart from small variations. The lack of any noticeable quantum mechanical difference between the Si atoms in the core and those at the surface (the Si-H interface) makes it easier to apply continuum modeling successfully to the hydrogen-passivated wires. As we consider how these effects transfer to other kinds of wires, the extrinsic surface effect coming from the surface adsorbates will require a careful treatment, and in cases where the surface interactions are stronger it may prove more difficult for continuum models to provide an accurate description of small wires.

The calculations presented here are at absolute zero temperature. Given the present-day computers, it is not possible to carry out these first-principles calculations at finite temperature. Based on the results of empirical molecular dynamics,[9,10,16] the general form of the size dependence of the Young's modulus is expected to be retained at finite temperatures well below the melt point, but the value of the modulus will change. Naturally, thermal softening will shift the entire curve, but also the value of the coefficient of the surface-area-to-volume ratio term will be somewhat temperature dependent. For this and many other applications it is desirable to construct classical interatomic potentials, whether quantum-based or strictly empirical, that capture the surface physics relevant to the mechanics of nanostructures.[26] First-principles calculations, such as those presented here, lay the groundwork for the development of those potentials. There is clearly much to be done in the development of Nanomechanics.

* Electronic address: robert.rudd@llnl.gov

[1] J. W. Cahn, Acta Metall. **28**, 1333 (1980).

[2] A. N. Cleland and M. L. Roukes, Appl. Phys. Lett. **69**, 2653 (1996).

[3] C. L. Cheung, J. H. Hafner, and C. M. Lieber, Proc. Natl. Acad. Sci. USA **97**, 3809 (2000).

[4] H. G. Craighead, Science **24**, 1532 (2000).

[5] D. Rugar, C. S. Yannoni, and J. A. Sidles, Nature (London) **360**, 563 (1992).

[6] S. D. Solares, M. Blanco, and W. A. Goddard, Nanotechnology **15**, 1405 (2004).

[7] A. N. Cleland and M. R. Geller, Phys. Rev. Lett. **93**, 070501 (2004).

[8] M. Blencowe, Phys. Rep. **395**, 159 (2004).

[9] J. Q. Broughton, C. A. Meli, P. Vashishta, and R. K. Kalia, Phys. Rev. B **56**, 611 (1997).

[10] R. E. Rudd and J. Q. Broughton, J. Mod. Sim. Microsys. **1**, 29 (1999).

[11] B. Lee and R. E. Rudd, Phys. Rev. B **75**, 041305(R) (2007).

[12] A. Gaidarzhy, G. Zolfagharkhani, R. L. Badzey, and P. Mohanty, Phys. Rev. Lett. **94**, 030402 (2005).

[13] C. M. Lieber, MRS Bull. **28**, 486 (2003).

[14] R. Rurali and N. Lorente, Phys. Rev. Lett. **94**, 026805 (2005).

[15] D. D. D. Ma, C. S. Lee, F. C. K. Au, S. Y. Tong, and S. T. Lee, Science **299**, 1874 (2003).

[16] R. E. Rudd, Int. J. Multiscale Comput. Eng. **2**, 203 (2004).

[17] R. E. Miller and V. B. Shenoy, Nanotechnology **11**, 139 (2000).

[18] M. E. Gurtin and A. I. Murdoch, Arch. Rat. Mech. Anal. **57**, 291 (1975).

[19] R. V. Kukta, D. Kouris, and K. Sieradzki, J. Mech. Phys. Solids **51**, 1243 (2003).

[20] H. S. Park, P. A. Klein, and G. J. Wagner, Int. J. Numer. Meth. Engng. **68**, 1072 (2006).

[21] A. F. da Fonseca, C. P. Malta, and D. S. Galvão, J. Appl. Phys. **99**, 094310 (2006).

[22] V. A. Shchukin, N. N. Ledentsov, P. S. Kop'ev, and D. Bimberg, Phys. Rev. Lett. **75**, 2968 (1995).

[23] R. E. Rudd, G. A. D. Briggs, A. P. Sutton, G. Medeiros-Ribeiro, and R. S. Williams, Phys. Rev. Lett. **90**, 146101 (2003).

[24] R. E. Rudd, G. A. D. Briggs, A. P. Sutton, G. Medeiros-Ribeiro, and R. S. Williams, to appear J. Comput. Theor. Nanosci. (2007).

[25] H. Liang, M. Upmanyu, and H. Huang, Phys. Rev. B **71**, 241403(R) (2005).

[26] B. Lee and K. Cho, Surf. Sci. **600**, 1982 (2006).

[27] H. Balamane, T. Halicioglu, and W. A. Tiller, Phys. Rev. B **46**, 2250 (1992).

[28] S. Ismail-Beigi and T. Arias, Phys. Rev. B **57**, 11923 (1998).

[29] E. W. Wong, P. E. Sheehan, and C. M. Lieber, Science **277**, 1971 (1997).

[30] S. Cuenot, C. Fretigny, S. Demoustier-Champagne, and B. Nysten, Phys. Rev. B **69**, 165410 (2004).

[31] C. Q. Chen, Y. Shi, Y. S. Zhang, J. Zhu, and Y. J. Yan, Phys. Rev. Lett. **96**, 075505 (2006).

[32] W. Q. Ding, L. Calabri, X. Q. Chen, K. M. Kohlhaas, and R. S. Ruoff, Composites Sci. Tech. **66**, 1109 (2006).

[33] L. T. Ngo *et al.*, Nano Lett. **6**, 2964 (2006).

[34] T. Kizuka, Y. Takatani, K. Asaka, and R. Yoshizaki, Phys. Rev. B **72**, 035333 (2005).

[35] A. San Paulo *et al.*, Appl. Phys. Lett. **87**, 053111 (2005).

[36] X. Li, T. Ono, Y. Wang, and M. Esashi, Appl. Phys. Lett. **83**, 3081 (2003).

[37] X. Q. Chen, S. L. Zhang, G. J. Wagner, W. Q. Ding, and R. S. Ruoff, J. Appl. Phys. **95**, 4823 (2004).

[38] J. Bernholc, D. Brenner, M. B. Nardelli, V. Meunier, and C. Roland, Annu. Rev. Mater. Res. **32**, 347 (2002).

[39] W. Kohn and L. J. Sham, Phys. Rev. A **140**, 1133 (1965).

[40] D. E. Segall, S. Ismail-Beigi, and T. A. Arias, Phys. Rev. B **65**, 214109 (2002).

[41] L. G. Zhou and H. Huang, Appl. Phys. Lett. **84**, 1940 (2004); L. Zhang and H. Huang, *ibid.* **89**, 183111 (2006).

[42] Y. Umeno, A. Kushima, T. Kitamura, P. Gumbsch, and J. Li, Phys. Rev. B **72**, 165431 (2005).

[43] J. Ihm and M. L. Cohen, Sol. Stat. Comm. **29**, 711 (1979).

[44] O. H. Nielsen and R. M. Martin, Phys. Rev. B **32**, 3792 (1985).

[45] J. Ihm, M. T. Yin, and M. L. Cohen, Sol. Stat. Comm. **37**, 491 (1981).

[46] P. E. Blöchl, Phys. Rev. B **50**, 17953 (1994).

[47] G. Kresse and D. Joubert, Phys. Rev. B **59**, 1758 (1999).

[48] J. P. Perdew, K. Burke, and M. Ernzerhof, Phys. Rev. Lett. **77**, 3865 (1996).

[49] H. J. Monkhorst and J. D. Pack, Phys. Rev. B **13**, 5188 (1976).

[50] H. J. McSkimin, J. Appl. Phys. **24**, 988 (1953); H. J. McSkimin and P. Andreatch, Jr, *ibid.* **35**, 2161 (1964).

[51] W. B. Gauster, Phys. Rev. B **4**, 1288 (1971).

[52] R. E. Schlier and H. E. Farnsworth, J. Chem. Phys. **30**, 917 (1959).

[53] D. J. Chadi, Phys. Rev. Lett. **43**, 43 (1979).

[54] A. A. Stekolnikov, J. Furthmüller, and F. Bechstedt, Phys. Rev. B **65**, 115318 (2002).

[55] T. Sakurai and H. D. Hagstrum, Phys. Rev. B **14**, 1593 (1976).

[56] J. E. Northrup, Phys. Rev. B **44**, 1419 (1991).

[57] R. D. Meade and D. Vanderbilt, Phys. Rev. Lett. **63**, 1404 (1989).

[58] D. Sander and H. Ibach, Phys. Rev. B **43**, 4263 (1991).

[59] K. Stokbro, E. Nielsen, E. Hult, Y. Andersson, and B. I. Lundqvist, Phys. Rev. B **58**, 16118 (1998).

[60] S. Garcia-Manyes, A. G. Güell, P. Gorostiza, and F. Sanz, J. Chem. Phys. **123**, 114711 (2005).

[61] R. Astala, M. Kaukonen, R. M. Nieminen, and T. Heine, Phys. Rev. B **61**, 2973 (2000).

[62] S. Ciraci and I. P. Batra, Surf. Sci. **178**, 80 (1986).

[63] See for example R. J. Needs, Phys. Rev. Lett. **58**, 53 (1987).

[64] See for example F. H. Streitz, R. C. Cammarata, and K. Sieradzki, Phys. Rev. B **49**, 10699 (1994).

[65] B. Lee and R. E. Rudd, in preparation.

[66] J. E. Pask, B. M. Klein, P. A. Sterne, and C. Y. Fong, Comput. Phys. Comm. **135**, 1 (2001).

[67] S. S. Verbridge, J. M. Parpia, R. B. Reichenbach, L. M. Bellan, and H. G. Craighead, J. Appl. Phys. **99**, 124304 (2006).

[68] D. G. Pettifor, Phys. Rev. Lett. **63**, 2480 (1989).

[69] J. A. Moriarty, Phys. Rev. B **42**, 1609 (1990).

[70] R. E. Rudd and B. Lee, in preparation.

[71] For clarity, we emphasize that the extrinsic contribution is included in the nanowire Young's modulus presented in this work.

[72] T. C. Au Yeung, *et al.*, Phys. Rev. B **74**, 155317 (2006).